Extensional, Thickness-Stretch and Symmetric Thickness-Shear Vibrations of Piezoceramic Disks

Rui Huang, Peter C. Y. Lee, *Member, IEEE*, Wen-Sen Lin, and Jiun-Der Yu, *Associate Member, IEEE*

Abstract—**A set of two-dimensional (2-D), second-order approximate equations for extensional, thickness-stretch and symmetric thickness-shear vibrations of piezoelectric ceramic plates with electroded faces is extracted from the infinite system of 2-D equations deduced previously. The new truncation procedure developed recently is used for it improves the accuracy of calculated dispersion curves. Closed-form solutions are obtained for free vibrations of circular disks of barium titanate. Dispersion curves calculated from the present approximate 2-D equations are compared with those obtained from the 3-D equations, and the predicted resonance frequencies are compared with experimental data. Both comparisons show good agreement without any corrections. The frequencies of the edge modes calculated from the present 2-D equations are very close to the experimental data. Furthermore, mode shapes at various frequencies are calculated in order to identify the frequency segments of the spectrum at which one of the coupled modes—i.e., the radial extension (R), edge mode (Eg), thickness-stretch (TSt), and symmetric thickness-shear (s.TSh)—is predominant.**

I. Introduction

In a previous paper [1], an infinite system of two-dimensional (2-D) equations for piezoelectric crystal plates with electroded faces was derived. The approximate first-order equations extracted from the infinite system were shown to give very accurate dispersion curves and frequency spectra for the vibrations of thickness-shear, flexural, and face-shear modes varying in the x_1 direction and thickness-twist and face-shear modes varying in the x_3 direction in rectangular AT-cut quartz plates. In a recent paper [2], an infinite system of 2-D equations for plates with charge-free faces was similarly obtained. The approximate second-order equations, extracted by a new truncation procedure, were shown to give very accurate dispersion curves and, consequently, very accurate frequency spectrum for the extensional, thickness-stretch and symmetric thickness-shear vibrations of piezoelectric crystal strips [2]. Free vibrations of piezoelectric ceramic actuators had been analyzed by Yu [3] using a system of second-order 2-D equations of extensional motion.

In the present paper, a set of second-order governing equations for piezoelectric crystal plates with electroded faces is obtained from the infinite system of 2-D equations in [1] by the new truncation procedure developed in [2]. Closed-form solutions are obtained for the extensional, thickness-stretch, and symmetric thickness-shear vibrations of circular disks of piezoelectric ceramics. Dispersion curves computed from the present 2-D equations for barium titanate ($BaTiO_3$) disks are compared with those from the 3-D equations, and predicted resonance frequencies are compared with the experimental data of Shaw [4].

Special attention is given to the edge mode, which was first discovered experimentally by Shaw [4] then investigated by Gazis and Mindlin [5]. The theoretical frequency spectrum in [5] was compared with Shaw's [4] experimental results with very good general agreement, except that the theoretical frequencies of the edge modes are lower than the experimental data by about 12%. From the present 2-D equations, the predicted frequencies of the edge modes agree closely with the experimental data, with the discrepancy less than 3%, and without using any correction factors. In many previous approximate 2-D equations, such as that in Gazis and Mindlin [5], correction factors were usually introduced in order to improve the accuracy of predicted dispersion relations of vibrations of the plate.

Mode shapes of the circular disks of $BaTiO_3$ are computed to determine the patterns of vibrations. The calculated displacement patterns of the extensional modes, edge modes, and thickness-stretch modes are compared with Shaw's [4] observations. The symmetric thickness-shear mode, which was not observed in Shaw's [4] experiments for thick $BaTiO_3$ disks, is shown to exist in the frequency spectrum for thin disks with large diameter-to-thickness ratios.

II. Two-Dimensional Equations

For the system of 2-D governing equations of piezoelectric crystal plates in [1], the thickness coordinate was designated by x_2. In this paper, we consider piezoelectric ceramic plates, for which the thickness coordinate is in the poling direction of the ceramics and is designated by x_3, as shown in Fig. 1. After transferring the thickness coordinate

Manuscript received October 29, 2001; accepted April 7, 2002. This work was supported by Grant No. DAAH 04-95-1-0614 and No. DAAH 04-95-1-0102 from the U.S. Army Research Office.

R. Huang and P. C. Y. Lee are with the Department of Civil and Environmental Engineering, Princeton University, Princeton, NJ 08544 (e-mail: lee@princeton.edu).

W. S. Lin is with the AT&T R&D Headquarters, Middletown, NJ 07748.

J. D. Yu is with the Epson Palo Alto Lab, Palo Alto, CA 94304.

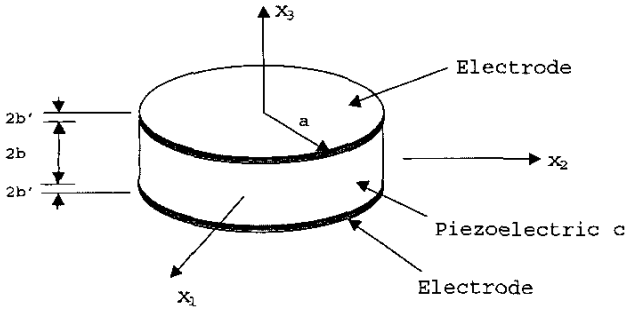

Fig. 1. A piezoelectric ceramic disk with electroded faces.

from x_2 to x_3, the 2-D equations in [1] are summarized as follows.

Series expansion of displacement and electric potential:

$$\begin{aligned} u_i(x_1,x_2,x_3,t) &= -u_{3,i}^{(0)}(x_1,x_2,t)x_3 \\ &\quad + \sum_{n=0}^{\infty} u_i^{(n)}(x_1,x_2,t)\cos\frac{n\pi}{2}(1-\psi), \\ \phi(x_1,x_2,x_3,t) &= \bar{V}_0(t) + \bar{V}_1(t)\psi \\ &\quad + \sum_{n=0}^{\infty} \phi^{(n)}(x_1,x_2,t)\sin\frac{n\pi}{2}(1-\psi), \end{aligned} \tag{1}$$

where $\psi = x_3/b$ and $\bar{V}_0$, $\bar{V}_1$ are determined by the specified electric potentials at the electroded faces.

Strain and electric field:

$$\begin{aligned} S_{ij} &= S_{ij}^d\psi + \sum_{n=0}^{\infty}\left[S_{ij}^{(n)}\cos\frac{n\pi}{2}(1-\psi) + \bar{S}_{ij}^{(n)}\sin\frac{n\pi}{2}(1-\psi)\right], \\ E_i &= \sum_{n=0}^{\infty}\left[E_i^{(n)}\sin\frac{n\pi}{2}(1-\psi) + \bar{E}_i^{(n)}\cos\frac{n\pi}{2}(1-\psi)\right], \end{aligned} \tag{2}$$

where

$$\begin{aligned} S_{ij}^d &= -bu_{3,ij}^{(0)}, \\ S_{ij}^{(n)} &= \frac{1}{2}\left[u_{i,j}^{(n)} + u_{j,i}^{(n)} - \delta_{0n}(\delta_{3i}u_{3,j}^{(0)} + \delta_{3j}u_{3,i}^{(0)})\right], \\ \bar{S}_{ij}^{(n)} &= \frac{n\pi}{4b}\left(\delta_{3i}u_j^{(n)} + \delta_{3j}u_i^{(n)}\right), \\ E_i^{(n)} &= -\phi_{,i}^{(n)}, \\ \bar{E}_i^{(n)} &= \delta_{3i}\left(\frac{n\pi}{2b}\phi^{(n)} - \delta_{0n}\frac{\bar{V}_1}{b}\right). \end{aligned} \tag{3}$$

Field equations:

$$\begin{aligned} T_{ij,i}^{(n)} - \frac{n\pi}{2b}\bar{T}_{3j}^{(n)} + \frac{1}{b}F_j^{(n)} &= (1+\delta_{n0})\,\rho\ddot{u}_j^{(n)} - c_n\rho b\ddot{u}_{3,j}^{(0)}, \\ \bar{D}_{a,a}^{(n)} + \frac{n\pi}{2b}D_3^{(n)} &= 0, \end{aligned} \tag{4}$$

where $n = 0, 1, 2, \cdots$, $a = 1, 2$, and

$$F_j^{(n)} = T_{3j}(x_3 = b) - (-1)^n T_{3j}(x_3 = -b). \tag{5}$$

Constitutive equations:

$$\begin{aligned} T_{ij}^d &= \frac{2}{3}c_{ijkl}S_{kl}^d + \sum_{m=0}^{\infty} \\ &\quad \left[c_m(c_{ijkl}S_{kl}^{(m)} - e_{kij}\bar{E}_k^{(m)}) + s_m(c_{ijkl}\bar{S}_{kl}^{(m)} - e_{kij}E_k^{(m)})\right], \\ T_{ij}^{(n)} &= c_n c_{ijkl}S_{kl}^d + (1+\delta_{0n})(c_{ijkl}S_{kl}^{(n)} - e_{kij}\bar{E}_k^{(n)}) \\ &\quad + \sum_{m=0}^{\infty} B_{mn}(c_{ijkl}\bar{S}_{kl}^{(m)} - e_{kij}E_k^{(m)}), \\ \bar{T}_{ij}^{(n)} &= s_n c_{ijkl}S_{kl}^d + (1-\delta_{0n})(c_{ijkl}\bar{S}_{kl}^{(n)} - e_{kij}E_k^{(n)}) \\ &\quad + \sum_{m=0}^{\infty} B_{nm}(c_{ijkl}S_{kl}^{(m)} - e_{kij}\bar{E}_k^{(m)}), \\ D_i^{(n)} &= c_n e_{ijk}S_{jk}^d + (1+\delta_{0n})(e_{ijk}S_{jk}^{(n)} + \epsilon_{ij}\bar{E}_j^{(n)}) \\ &\quad + \sum_{m=0}^{\infty} B_{mn}(e_{ijk}\bar{S}_{jk}^{(m)} + \epsilon_{ij}E_j^{(m)}), \\ \bar{D}_i^{(n)} &= s_n e_{ijk}S_{jk}^d + (1-\delta_{0n})(e_{ijk}\bar{S}_{jk}^{(n)} + \epsilon_{ij}E_j^{(n)}) \\ &\quad + \sum_{m=0}^{\infty} B_{nm}(e_{ijk}S_{jk}^{(m)} + \epsilon_{ij}\bar{E}_j^{(m)}), \end{aligned} \tag{6}$$

where

$$\begin{aligned} c_n &= \int_{-1}^{1}\psi\cos\frac{n\pi}{2}(1-\psi)d\psi = \begin{cases} \dfrac{8}{n^2\pi^2}, & n = \text{odd} \\ 0, & n = \text{even} \end{cases} \\ s_n &= \int_{-1}^{1}\psi\sin\frac{n\pi}{2}(1-\psi)d\psi = \begin{cases} \dfrac{4}{n\pi}, & n = 2,4,6,\cdots \\ 0, & n = 0,1,3,5,\cdots \end{cases} \\ B_{mn} &= \int_{-1}^{1}\sin\frac{m\pi}{2}(1-\psi)\cos\frac{n\pi}{2}(1-\psi)d\psi \\ &= \begin{cases} \dfrac{4m}{(m^2-n^2)\pi}, & m+n = \text{odd} \\ 0, & m+n = \text{even}. \end{cases} \end{aligned} \tag{7}$$

Edge conditions to be specified:

$$\begin{aligned} t_3^{(0)} + bt_{s,s}^d = T_{3\nu}^{(0)} + bT_{\nu s,s}^d, &\quad \text{or } u_3^{(0)} = \hat{u}_3^{(0)}, \\ t_\nu^d = T_{\nu\nu}^d, &\quad \text{or } u_{3,\nu}^{(0)} = \hat{u}_{3,\nu}^{(0)}, \\ t_a^{(0)} = \nu_i T_{ia}^{(0)}, &\quad \text{or } u_a^{(0)} = \hat{u}_a^{(0)}, \\ t_j^{(m)} = \nu_i T_{ij}^{(m)}, &\quad \text{or } u_j^{(m)} = \hat{u}_j^{(m)}, \\ \bar{\sigma}^{(m)} = \nu_i \bar{D}_i^{(m)}, &\quad \text{or } \phi^{(m)} = \hat{\phi}^{(m)}, \end{aligned} \tag{8}$$

where the capped quantities are specified values on edge, s and ν are unit vectors tangential and normal to the edge, respectively, $a = 1, 2$, $m = 1, 2, 3, \cdots$, and

$$\begin{aligned} t_i^d &= \int_{-1}^{1} t_i\psi d\psi, \\ t_i^{(n)} &= \int_{-1}^{1} t_i\cos\frac{n\pi}{2}(1-\psi)d\psi, \\ \bar{\sigma}^{(n)} &= \int_{-1}^{1}\sigma\sin\frac{n\pi}{2}(1-\psi)d\psi, \end{aligned} \tag{9}$$

in which t_i and σ are the surface traction and the surface charge density, respectively.

III. Second-Order Equations

To extract a finite set of second-order approximate equations from the infinite system of 2-D equations in the previous section, we let:

$$\begin{aligned} &u_j^{(n)} = 0,\ n > 2 \text{ except } u_3^{(3)},\ u_1^{(4)},\ u_2^{(4)},\\ &\phi^{(n)} = 0,\ n > 2,\\ &\ddot{u}_3^{(3)} = \ddot{u}_1^{(4)} = \ddot{u}_2^{(4)} = 0,\\ &\bar{T}_{33}^{(3)} = \bar{T}_{31}^{(4)} = \bar{T}_{32}^{(4)} = 0. \end{aligned} \tag{10}$$

and disregard $T_{ij}^{(n)}$, $\bar{T}_{ij}^{(n)}$ and $D_i^{(n)}$, $\bar{D}_i^{(n)}$ for $n > 2$. The new truncation procedure developed in [2] is used in (10), where $u_3^{(3)}$, $u_1^{(4)}$, $u_2^{(4)}$ are allowed for free development; but in the previous truncation for second-order equations only $u_3^{(3)}$ is permitted for free development.

Accordingly, the infinite number of field equations in (4) reduce to:

$$\begin{aligned} &T_{ij,i}^{(0)} + \frac{1}{b}F_j^{(0)} = 2\rho\ddot{u}_j^{(0)},\\ &T_{ij,i}^{(1)} - \frac{\pi}{2b}\bar{T}_{3j}^{(1)} + \frac{1}{b}F_j^{(1)} = \rho\ddot{u}_j^{(1)} - \frac{8}{\pi^2}\rho b\ddot{u}_{3,j}^{(0)},\\ &T_{ij,i}^{(2)} - \frac{\pi}{b}\bar{T}_{3j}^{(2)} + \frac{1}{b}F_j^{(2)} = \rho\ddot{u}_j^{(2)},\\ &\bar{D}_{a,a}^{(1)} + \frac{\pi}{2b}D_3^{(1)} = 0,\\ &\bar{D}_{a,a}^{(2)} + \frac{\pi}{b}D_3^{(2)} = 0, \end{aligned} \tag{11}$$

where $i, j = 1, 2, 3$ and $a = 1, 2$.

The mechanical strain-displacement relations and the electric field-potential relations are obtained from (3). Associated with the higher order displacements $u_3^{(3)}$, $u_1^{(4)}$, $u_2^{(4)}$, we have:

$$\bar{S}_3^{(3)} = \frac{3\pi}{2b}u_3^{(3)}, \quad \bar{S}_4^{(4)} = \frac{2\pi}{b}u_2^{(4)}, \quad \bar{S}_5^{(4)} = \frac{2\pi}{b}u_1^{(4)}, \tag{12}$$

which can be solved from the constitutive equations (6) by setting $\bar{T}_{33}^{(3)}$, $\bar{T}_{31}^{(4)}$, $\bar{T}_{32}^{(4)}$ to zero, i.e.:

$$\begin{aligned} \bar{S}_3^{(3)} &= -\frac{1}{c_{33}} \left[\frac{4}{3\pi}(c_{3q}S_q^{(0)} - e_{k3}\bar{E}_k^{(0)}) + \frac{12}{5\pi}(c_{3q}S_q^{(2)} - e_{k3}\bar{E}_k^{(2)})\right],\\ \bar{S}_4^{(4)} &= -\frac{1}{c_{44}}\left[\frac{1}{\pi}c_{4q}S_q^d + \frac{16}{15\pi}(c_{4q}S_q^{(1)} - e_{k4}\bar{E}_k^{(1)})\right],\\ \bar{S}_5^{(4)} &= -\frac{1}{c_{55}}\left[\frac{1}{\pi}c_{5q}S_q^d + \frac{16}{15\pi}(c_{5q}S_q^{(1)} - e_{k5}\bar{E}_k^{(1)})\right]. \end{aligned} \tag{13}$$

Substitution of (13) into the remaining relations of (6) eliminates $\bar{S}_3^{(3)}$, $\bar{S}_4^{(4)}$, $\bar{S}_5^{(4)}$ from the constitutive equations, and thus $u_3^{(3)}$, $u_1^{(4)}$, $u_2^{(4)}$ from the second-order equations. The modified constitutive equations for second-order equations are obtained as:

$$\begin{aligned} T_p^{(0)} &= 2(c_{pq}^{(0)}S_q^{(0)} - e_{kp}^{(0)}\bar{E}_k^{(0)}) + \frac{4}{\pi}(c_{pq}\bar{S}_q^{(1)} - e_{kp}E_k^{(1)})\\ &\quad - (c_{pq}^{(3)}S_q^{(2)} - e_{kp}^{(3)}\bar{E}_k^{(2)}),\\ T_p^{(1)} &= \frac{8}{\pi^2}c_{pq}^d S_q^d + (c_{pq}^{(1)}S_q^{(1)} - e_{kp}^{(1)}\bar{E}_k^{(1)})\\ &\quad + \frac{8}{3\pi}(c_{pq}\bar{S}_q^{(2)} - e_{kp}E_k^{(2)}),\\ T_p^{(2)} &= (c_{pq}^{(2)}S_q^{(2)} - e_{kp}^{(2)}\bar{E}_k^{(2)}) - \frac{4}{3\pi}(c_{pq}\bar{S}_q^{(1)} - e_{kp}E_k^{(1)})\\ &\quad - (c_{pq}^{(3)}S_q^{(0)} - e_{kp}^{(3)}\bar{E}_k^{(0)}),\\ \bar{T}_p^{(1)} &= c_{pq}\bar{S}_q^{(1)} - e_{kp}E_k^{(1)} + \frac{4}{\pi}(c_{pq}S_q^{(0)} - e_{kp}\bar{E}_k^{(0)})\\ &\quad - \frac{4}{3\pi}(c_{pq}S_q^{(2)} - e_{kp}\bar{E}_k^{(2)}),\\ \bar{T}_p^{(2)} &= \frac{2}{\pi}c_{pq}S_q^d + (c_{pq}\bar{S}_q^{(2)} - e_{kp}E_k^{(2)})\\ &\quad + \frac{8}{3\pi}(c_{pq}S_q^{(1)} - e_{kp}\bar{E}_k^{(1)}),\\ D_i^{(0)} &= 2(e_{ip}^{(0)}S_p^{(0)} + \epsilon_{ij}^{(0)}\bar{E}_j^{(0)}) + \frac{4}{\pi}(e_{ip}\bar{S}_p^{(1)} + \epsilon_{ij}E_j^{(1)})\\ &\quad - (e_{ip}^{(3)}S_p^{(2)} - \epsilon_{ij}^{(3)}\bar{E}_j^{(2)}),\\ D_i^{(1)} &= \frac{8}{\pi^2}e_{ip}^d S_p^d + (e_{ip}^{(1)}S_p^{(1)} + \epsilon_{ij}^{(1)}\bar{E}_j^{(1)})\\ &\quad + \frac{8}{3\pi}(e_{ip}\bar{S}_p^{(2)} + \epsilon_{ij}E_j^{(2)}),\\ D_i^{(2)} &= (e_{ip}^{(2)}S_p^{(2)} + \epsilon_{ij}^{(2)}\bar{E}_j^{(2)}) - \frac{4}{3\pi}(e_{ip}\bar{S}_p^{(1)} + \epsilon_{ij}E_j^{(1)})\\ &\quad - (e_{ip}^{(3)}S_p^{(0)} - \epsilon_{ij}^{(3)}\bar{E}_j^{(0)}),\\ \bar{D}_i^{(1)} &= (e_{ip}\bar{S}_p^{(1)} + \epsilon_{ij}E_j^{(1)}) + \frac{4}{\pi}(e_{ip}S_p^{(0)} + \epsilon_{ij}\bar{E}_j^{(0)})\\ &\quad - \frac{4}{3\pi}(e_{ip}S_p^{(2)} + \epsilon_{ij}\bar{E}_j^{(2)}),\\ \bar{D}_i^{(2)} &= \frac{2}{\pi}e_{ip}S_p^d + (e_{ip}\bar{S}_p^{(2)} + \epsilon_{ij}E_j^{(2)})\\ &\quad + \frac{8}{3\pi}(e_{ip}S_p^{(1)} + \epsilon_{ij}\bar{E}_j^{(1)}), \end{aligned} \tag{14}$$

where

$$c_{pq}^d = c_{pq} - \frac{2}{15}\left(\frac{c_{p4}c_{4q}}{c_{44}} + \frac{c_{p5}c_{5q}}{c_{55}}\right), \tag{15a}$$

$$e_{kp}^d = e_{kp} - \frac{2}{15}\left(\frac{c_{p4}e_{k4}}{c_{44}} + \frac{c_{p5}e_{k5}}{c_{55}}\right), \tag{15b}$$

$$c_{pq}^{(0)} = c_{pq} - \frac{8}{9\pi^2}\frac{c_{p3}c_{3q}}{c_{33}}, \tag{15c}$$

$$e_{kp}^{(0)} = e_{kp} - \frac{8}{9\pi^2}\frac{c_{p3}e_{k3}}{c_{33}}, \tag{15d}$$

$$c_{pq}^{(1)} = c_{pq} - \frac{256}{225\pi^2}\left(\frac{c_{p4}c_{4q}}{c_{44}} + \frac{c_{p5}c_{5q}}{c_{55}}\right), \tag{15e}$$

$$e_{kp}^{(1)} = e_{kp} - \frac{256}{225\pi^2}\left(\frac{c_{p4}e_{k4}}{c_{44}} + \frac{c_{p5}e_{k5}}{c_{55}}\right), \tag{15f}$$

$$c_{pq}^{(2)} = c_{pq} - \frac{144}{25\pi^2}\frac{c_{p3}c_{3q}}{c_{33}}, \tag{15g}$$

$$e_{kp}^{(2)} = e_{kp} - \frac{144}{25\pi^2}\frac{c_{p3}e_{k3}}{c_{33}}, \tag{15h}$$

$$c_{pq}^{(3)} = \frac{16}{5\pi^2}\frac{c_{p3}c_{3q}}{c_{33}}, \tag{15i}$$

$$e_{kp}^{(3)} = \frac{16}{5\pi^2}\frac{c_{p3}e_{k3}}{c_{33}}, \tag{15j}$$

$$\epsilon_{ij}^{(0)} = \epsilon_{ij} + \frac{8}{9\pi^2}\frac{e_{i3}e_{j3}}{c_{33}}, \tag{15k}$$

$$\epsilon_{ij}^{(1)} = \epsilon_{ij} + \frac{256}{225\pi^2}\left(\frac{e_{i4}e_{j4}}{c_{44}} + \frac{e_{i5}e_{j5}}{c_{55}}\right), \tag{15l}$$

$$\epsilon_{ij}^{(2)} = \epsilon_{ij} + \frac{144}{25\pi^2}\frac{e_{i3}e_{j3}}{c_{33}}, \tag{15m}$$

$$\epsilon_{ij}^{(3)} = \frac{16}{5\pi^2}\frac{e_{i3}e_{j3}}{c_{33}}. \tag{15n}$$

The effect of inertial forces of the symmetrically plated thin electrodes, which have mass density ρ' and thickness $2b'$ ($b' \ll b$), can be taken into account in the face tractions in (5) by letting:

$$\begin{aligned} F_j^{(n)} &= \mathcal{F}_j^{(n)} - 4b'\rho'(\ddot{u}_j^{(0)} + \ddot{u}_j^{(2)}), \quad \text{for } n = 0, 2, \cdots, \\ F_j^{(n)} &= \mathcal{F}_j^{(n)} - 4b'\rho'(\ddot{u}_j^{(1)} - \ddot{u}_{3,j}^{(0)} b) \quad \text{for } n = 1, 3, \cdots, \end{aligned} \tag{16}$$

where

$$\mathcal{F}_j^{(n)} = T_{3j}(x_3 = b + 2b') - (-1)^n T_{3j}(x_3 = -b - 2b'). \tag{17}$$

Hence, the second-order governing equations for piezoelectric crystal plates with electroded faces can be obtained by substituting (16) into (11). For piezoelectric ceramic plates, constitutive equations (14) are greatly reduced for the material symmetry of polarized ferroelectric ceramics. Substitution of these reduced relations into (11) leads to the second-order governing equations of mechanical displacements and electric potentials:

$$\begin{aligned} &(c_{11}^{(0)} + c_{12}^{(0)})\nabla(\nabla\cdot\mathbf{u}_T^{(0)}) + 2c_{66}\nabla^2\mathbf{u}_T^{(0)} + \frac{2}{b}c_{13}\nabla u_3^{(1)} \\ &\quad - c_{11}^{(3)}\nabla(\nabla\cdot\mathbf{u}_T^{(2)}) + \frac{\pi}{b}e_{31}^{(3)}\nabla\phi^{(2)} + \frac{1}{b}\mathbf{F}_T^{(0)} \\ &\quad = 2(1+R)\rho\ddot{\mathbf{u}}_T^{(0)} + 2R\rho\ddot{\mathbf{u}}_T^{(2)}, \end{aligned} \tag{18a}$$

$$\begin{aligned} &\frac{2}{b}c_{55}\nabla\cdot\mathbf{u}_T^{(1)} + \frac{4}{\pi}e_{15}\nabla^2\phi^{(1)} + \frac{1}{b}\mathcal{F}_3^{(0)} \\ &\quad = 2(1+R)\rho\ddot{u}_3^{(0)} + 2R\rho\ddot{u}_3^{(2)}, \end{aligned} \tag{18b}$$

$$\begin{aligned} &\frac{c_{11}+c_{12}}{2}\nabla(\nabla\cdot\mathbf{u}_T^{(1)}) + c_{66}\nabla^2\mathbf{u}_T^{(1)} - \frac{8b}{\pi^2}c_{11}\nabla^2(\nabla u_3^{(0)}) \\ &\quad + \frac{2}{3b}(4c_{13}+c_{55})\nabla u_3^{(2)} - \frac{\pi^2}{4b^2}c_{55}\mathbf{u}_T^{(1)} \\ &\quad - \frac{\pi}{2b}(e_{31}+e_{15})\nabla\phi^{(1)} + \frac{1}{b}\mathbf{F}_T^{(1)} \\ &\quad = (1+2R)\rho\ddot{\mathbf{u}}_T^{(1)} - (\frac{8}{\pi^2}+2R)\rho b\nabla\ddot{u}_3^{(0)}, \end{aligned} \tag{18c}$$

$$\begin{aligned} &c_{55}^{(1)}\nabla^2 u_3^{(1)} - \frac{2}{b}c_{13}\nabla\cdot\mathbf{u}_T^{(0)} + \frac{2}{3b}(c_{13}+4c_{55})\nabla\cdot\mathbf{u}_T^{(2)} \\ &\quad - \frac{\pi^2}{4b^2}c_{33}u_3^{(1)} + \frac{8}{3\pi}e_{15}\nabla^2\phi^{(2)} - \frac{2\pi}{3b^2}e_{33}\phi^{(2)} \\ &\quad - \frac{2}{b^2}e_{33}\bar{V}_1 + \frac{1}{b}\mathcal{F}_3^{(1)} = (1+2R)\rho\ddot{u}_3^{(1)}, \end{aligned} \tag{18d}$$

$$\begin{aligned} &\frac{c_{11}^{(2)}+c_{12}^{(2)}}{2}\nabla(\nabla\cdot\mathbf{u}_T^{(2)}) + c_{66}\nabla^2\mathbf{u}_T^{(2)} - c_{11}^{(3)}\nabla^2\mathbf{u}_T^{(0)} \\ &\quad - \frac{2}{3b}(c_{13}+4c_{55})\nabla u_3^{(1)} - \frac{\pi^2}{b^2}c_{55}\mathbf{u}_T^{(2)} \\ &\quad - \frac{\pi}{b}(e_{31}^{(2)}+e_{15})\nabla\phi^{(2)} + \frac{1}{b}\mathbf{F}_T^{(2)} = (1+2R)\rho\ddot{\mathbf{u}}_T^{(2)} + 2R\rho\ddot{\mathbf{u}}_T^{(0)}, \end{aligned} \tag{18e}$$

$$\begin{aligned} &2c_{13}\nabla^2 u_3^{(0)} + c_{55}\nabla^2 u_3^{(2)} - \frac{2}{3b}(c_{55}+4c_{13})\nabla\cdot\mathbf{u}_T^{(1)} \\ &\quad - \frac{\pi^2}{b^2}c_{33}u_3^{(2)} - \frac{4}{3\pi}e_{15}\nabla^2\phi^{(1)} + \frac{4\pi}{3b^2}e_{33}\phi^{(1)} \\ &\quad + \frac{1}{b}\mathcal{F}_3^{(2)} = (1+2R)\rho\ddot{u}_3^{(2)} + 2R\rho\ddot{u}_3^{(0)}, \end{aligned} \tag{18f}$$

$$\begin{aligned} &\frac{\pi}{2b}(e_{15}+e_{31})\nabla\cdot\mathbf{u}_T^{(1)} - \frac{4}{\pi}e_{31}\nabla^2 u_3^{(0)} - \frac{4}{3\pi}e_{15}\nabla^2 u_3^{(2)} \\ &\quad + \frac{4\pi}{3b^2}e_{33}u_3^{(2)} - \epsilon_{11}\nabla^2\phi^{(1)} + \frac{\pi^2}{4b^2}\epsilon_{33}\phi^{(1)} = 0, \end{aligned} \tag{18g}$$

$$\begin{aligned} &\frac{\pi}{b}(e_{15}+e_{31}^{(2)})\nabla\cdot\mathbf{u}_T^{(2)} - \frac{\pi}{b}e_{31}^{(3)}\nabla\cdot\mathbf{u}_T^{(0)} + \frac{8}{3\pi}e_{15}\nabla^2 u_3^{(1)} \\ &\quad - \frac{2\pi}{3b^2}e_{33}u_3^{(1)} - \epsilon_{11}\nabla^2\phi^{(2)} + \frac{\pi^2}{b^2}\epsilon_{33}^{(2)}\phi^{(2)} \\ &\quad - \frac{\pi}{b^2}\epsilon_{33}^{(3)}\bar{V}_1 = 0, \end{aligned} \tag{18h}$$

where

$$\begin{aligned} \mathbf{u}_T^{(n)} &= u_1^{(n)}\mathbf{e}_1 + u_2^{(n)}\mathbf{e}_2, \\ \mathbf{F}_T^{(n)} &= \mathcal{F}_1^{(n)}\mathbf{e}_1 + \mathcal{F}_2^{(n)}\mathbf{e}_2, \\ \nabla &= \mathbf{e}_1\frac{\partial}{\partial x_1} + \mathbf{e}_2\frac{\partial}{\partial x_2}, \\ R &= \frac{2\rho' b'}{\rho b}. \end{aligned} \tag{19}$$

It may be seen that (18) is separated into two coupled groups: (18a), (18d), (18e), and (18h) govern the symmetric vibrations of extensional ($\mathbf{u}_T^{(0)}$), thickness-stretch ($u_3^{(1)}$), and symmetric thickness-shear ($\mathbf{u}_T^{(2)}$) modes and potential $\phi^{(2)}$; and (18b), (18c), (18f) and (18g) govern the antisymmetric vibrations of flexural ($u_3^{(0)}$), antisymmetric thickness-shear ($\mathbf{u}_T^{(1)}$), and second-order thickness-stretch ($u_3^{(2)}$) modes and potential $\phi^{(1)}$. For the remainder of this paper, the first group of equations will be used to study the extensional (E), thickness-stretch (TSt) and symmetric thickness-shear (s.TSh) vibrations in circular disks of piezoelectric ceramics.

IV. Dispersion Relation

By setting $\mathbf{F}_T^{(0)}$, $\mathcal{F}_3^{(1)}$,$\mathbf{F}_T^{(2)}$, and $\bar{V}_1$ to zero in (18a), (18d), (18e), and (18h) for free vibrations of ceramic plates

with traction-free and shorted faces and taking the divergence of (18a) and (18e), we obtain:

$$
\begin{aligned}
&2c_{11}^{(0)}\nabla^2(\nabla\cdot\mathbf{u}_T^{(0)}) - c_{11}^{(3)}\nabla^2(\nabla\cdot\mathbf{u}_T^{(2)}) + \frac{2}{b}c_{13}\nabla^2 u_3^{(1)} \\
&\quad + \frac{\pi}{b}e_{31}^{(3)}\nabla^2\phi^{(2)} = 2(1+R)\rho\nabla\cdot\ddot{\mathbf{u}}_T^{(0)} + 2R\rho\nabla\cdot\ddot{\mathbf{u}}_T^{(2)}, \\
&c_{55}^{(1)}\nabla^2 u_3^{(1)} - \frac{2}{b}c_{13}\nabla\cdot\mathbf{u}_T^{(0)} + \frac{2}{3b}(c_{13}+4c_{55})\nabla\cdot\mathbf{u}_T^{(2)} \\
&\qquad - \frac{\pi^2}{4b^2}c_{33}u_3^{(1)} + \frac{8}{3\pi}e_{15}\nabla^2\phi^{(2)} \\
&\qquad - \frac{2\pi}{3b^2}e_{33}\phi^{(2)} = (1+2R)\rho\ddot{u}_3^{(1)}, \\
&c_{11}^{(2)}\nabla^2(\nabla\cdot\mathbf{u}_T^{(2)}) - c_{11}^{(3)}\nabla^2(\nabla\cdot\mathbf{u}_T^{(0)}) - \frac{2}{3b}(c_{13}+4c_{55})\nabla^2 u_3^{(1)} \\
&\qquad - \frac{\pi^2}{b^2}c_{55}\nabla\cdot\mathbf{u}_T^{(2)} - \frac{\pi}{b}(e_{31}^{(2)}+e_{15})\nabla^2\phi^{(2)} \\
&\qquad = (1+2R)\rho\nabla\cdot\ddot{\mathbf{u}}_T^{(2)} + 2R\rho\nabla\cdot\ddot{\mathbf{u}}_T^{(0)}, \\
&\frac{\pi}{b}(e_{15}+e_{31}^{(2)})\nabla\cdot\mathbf{u}_T^{(2)} - \frac{\pi}{b}e_{31}^{(3)}\nabla\cdot\mathbf{u}_T^{(0)} + \frac{8}{3\pi}e_{15}\nabla^2 u_3^{(1)} \\
&\qquad - \frac{2\pi}{3b^2}e_{33}u_3^{(1)} - \epsilon_{11}\nabla^2\phi^{(2)} + \frac{\pi^2}{b^2}\epsilon_{33}^{(2)}\phi^{(2)} = 0. \qquad (20)
\end{aligned}
$$

For axisymmetric vibrations of circular disks, we let:

$$
\begin{aligned}
\nabla\cdot\mathbf{u}_T^{(0)} &= \frac{1}{b}A_1 J_0(\xi r)e^{i\omega t}, \\
u_3^{(1)} &= A_2 J_0(\xi r)e^{i\omega t}, \\
\nabla\cdot\mathbf{u}_T^{(2)} &= \frac{1}{b}A_3 J_0(\xi r)e^{i\omega t}, \\
\phi^{(2)} &= \sqrt{\frac{c_{55}}{\epsilon_{33}}}A_4 J_0(\xi r)e^{i\omega t}.
\end{aligned} \qquad (21)
$$

Upon substituting (21) into (20), we obtain:

$$
\sum_{j=1}^{4} Q_{ij}(X;\Omega)A_j = 0, \qquad i,j = 1,2,3,4, \qquad (22)
$$

where the matrix Q_{ij} is given in (23) (see next page) and

$$
\begin{aligned}
&\Omega = \frac{\omega}{\frac{\pi}{2b}\sqrt{\frac{c_{55}}{\rho}}}, \qquad X = \frac{\xi}{\frac{\pi}{2b}}, \\
&R_1 = 1+R, \qquad R_2 = 1+2R, \\
&\tilde{c}_{pq} = \frac{c_{pq}}{c_{55}}, \qquad \tilde{e}_{kp} = \frac{e_{kp}}{\sqrt{c_{55}\epsilon_{33}}}, \qquad \tilde{\epsilon}_{ij} = \frac{\epsilon_{ij}}{\epsilon_{33}}, \qquad (24) \\
&\tilde{c}_{pq}^{(n)} = \frac{c_{pq}^{(n)}}{c_{55}}, \qquad \tilde{e}_{kp}^{(n)} = \frac{e_{kp}^{(n)}}{\sqrt{c_{55}\epsilon_{33}}}, \qquad \tilde{\epsilon}_{ij}^{(n)} = \frac{\epsilon_{ij}^{(n)}}{\epsilon_{33}}.
\end{aligned}
$$

For nontrivial solutions, we have

$$
\det\left[Q_{ij}(X;\Omega)\right] = 0, \qquad (25)
$$

which gives the dispersion relation for E-TSt-s.TSh vibrations of an infinite circular disk of piezoelectric ceramics.

It may be seen that, for a given value of frequency Ω, (25) gives four roots in wave number:

$$
X_j = \frac{\xi_j}{\frac{\pi}{2b}}, \qquad j = 1,2,3,4. \qquad (26)
$$

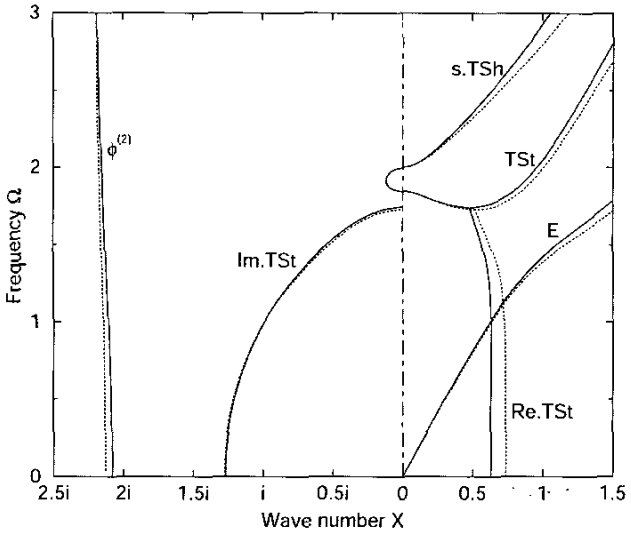

Fig. 2. Comparison of dispersion curves for E-TSt-s.TSh vibrations of a $BaTiO_3$ ceramic disk. Solid lines are from 2-D equations, and dotted lines are from 3-D equations, for $R = 0$.

Dispersion curves are calculated from (25) for $BaTiO_3$ disks with $R = 0$, and they are shown by solid lines in Fig. 2. The material properties of $BaTiO_3$ are taken from [6]. For comparison, dispersion curves also are calculated from the 3-D equations of linear piezoelectricity for straight-crested waves in an infinite plate, and they are shown in Fig. 2 by dotted lines. The complex branch of the TSt mode is represented by two lines for its real (Re) and imaginary (Im) parts, respectively. It is seen in Fig. 2 that the dispersion curves calculated from the present 2-D equations agree closely with those from the 3-D equations. We note that the new truncation procedure of [2] used in (10) has made significant improvement in accuracy of the dispersion curves without resorting to any correction factors. As it will be shown in Section V, the correct behavior of the TSt branch, especially in the vicinity of the cut-off frequency at the nonzero wave number (the intersection point of the real and complex segments of the TSt branch in Fig. 2), is crucial for predicting the correct frequencies of the edge modes. Similar observations was given in [5].

V. Frequency Spectrum

For the general solution of a finite disk, all four roots of (25) are needed in order to satisfy edge conditions. Hence, we let, for axisymmetric vibrations:

$$
\nabla\cdot\mathbf{u}_T^{(0)} = \frac{1}{b}\sum_{j=1}^{4}\alpha_{1j}B_j J_0(\xi_j r)e^{i\omega t}, \qquad (27a)
$$

$$
u_3^{(1)} = \sum_{j=1}^{4}\alpha_{2j}B_j J_0(\xi_j r)e^{i\omega t}, \qquad (27b)
$$

$$\begin{bmatrix} 2R_1\Omega^2 - 2\tilde{c}_{11}^{(0)}X^2 & -2\tilde{c}_{13}X^2 & 2R\Omega^2 + \tilde{c}_{11}^{(3)}X^2 & -\pi\tilde{e}_{31}^{(3)}X^2 \\ -2\tilde{c}_{13} & \frac{\pi^2}{4}(R_2\Omega^2 - \tilde{c}_{55}^{(1)}X^2 - \tilde{c}_{33}) & \frac{2}{3}(\tilde{c}_{13}+4) & -\frac{2\pi}{3}(\tilde{e}_{15}X^2 + \tilde{e}_{33}) \\ 2R\Omega^2 + \tilde{c}_{11}^{(3)}X^2 & \frac{2}{3}(\tilde{c}_{13}+4)X^2 & R_2\Omega^2 - \tilde{c}_{11}^{(2)}X^2 - 4 & \pi(\tilde{e}_{15} + \tilde{e}_{31}^{(2)})X^2 \\ -\tilde{e}_{31}^{(3)} & -\frac{2}{3}(\tilde{e}_{15}X^2 + \tilde{e}_{33}) & \tilde{e}_{15} + \tilde{e}_{31}^{(2)} & \frac{\pi}{4}(\tilde{\epsilon}_{11}X^2 + 4\tilde{\epsilon}_{33}^{(2)}) \end{bmatrix}, \tag{23}$$

$$\nabla \cdot \mathbf{u}_T^{(2)} = \frac{1}{b}\sum_{j=1}^{4} \alpha_{3j} B_j J_0(\xi_j r) e^{i\omega t}, \tag{27c}$$

$$\phi^{(2)} = \sqrt{\frac{c_{55}}{\epsilon_{33}}} \sum_{j=1}^{4} \alpha_{4j} B_j J_0(\xi_j r) e^{i\omega t}, \tag{27d}$$

where $B_j, j = 1, 2, 3, 4$ are the amplitudes to be determined from edge conditions and α_{kj} satisfy:

$$\sum_{k=1}^{4} Q_{ik}(X_j; \Omega)\alpha_{kj} = 0, \qquad i, j = 1, 2, 3, 4. \tag{28}$$

The components of displacement $u_r^{(0)}$ and $u_r^{(2)}$ are obtained by integrating (27a) and (27c):

$$\begin{aligned} u_r^{(0)} &= \sum_{j=1}^{4} \alpha_{1j} B_j \frac{J_1(\xi_j r)}{\xi_j b} e^{i\omega t}, \\ u_r^{(2)} &= \sum_{j=1}^{4} \alpha_{3j} B_j \frac{J_1(\xi_j r)}{\xi_j b} e^{i\omega t}. \end{aligned} \tag{29}$$

Edge conditions for circular disks are obtained by transforming (8) from Cartesian coordinates to cylindrical coordinates. Accordingly, for the second-order equations and axisymmetric vibrations of circular disks, the traction-free and charge-free edge conditions are

$$t_{rr}^{(0)} = t_{rr}^{(2)} = t_{rz}^{(1)} = \bar{\sigma}^{(2)} = 0, \qquad \text{at } r = a, \tag{30}$$

where a is the radius of the disk, and

$$\begin{aligned} t_{rr}^{(0)} &= 2\left(c_{12}^{(0)}\nabla \cdot \mathbf{u}_T^{(0)} + 2c_{66}\frac{\partial u_r^{(0)}}{\partial r}\right) - c_{11}^{(3)}\nabla \cdot \mathbf{u}_T^{(2)} \\ &\quad + \frac{2}{b}c_{13}u_3^{(1)} + \frac{\pi}{b}e_{31}^{(3)}\phi^{(2)} + 2e_{31}^{(0)}\frac{\bar{V}_1}{b}, \\ t_{rr}^{(2)} &= c_{12}^{(2)}\nabla \cdot \mathbf{u}_T^{(2)} + 2c_{66}\frac{\partial u_r^{(2)}}{\partial r} - c_{11}^{(3)}\nabla \cdot \mathbf{u}_T^{(0)} \\ &\quad - \frac{2}{3b}c_{13}u_3^{(1)} - \frac{\pi}{b}e_{31}^{(2)}\phi^{(2)} - e_{31}^{(3)}\frac{\bar{V}_1}{b}, \\ t_{rz}^{(1)} &= c_{55}^{(1)}\frac{\partial u_3^{(1)}}{\partial r} + \frac{8}{3b}c_{55}u_r^{(2)} + \frac{8}{3\pi}e_{15}\frac{\partial \phi^{(2)}}{\partial r}, \\ \bar{\sigma}^{(2)} &= \frac{\pi}{b}e_{15}u_r^{(2)} + \frac{8}{3\pi}e_{15}\frac{\partial u_3^{(1)}}{\partial r} - \epsilon_{11}\frac{\partial \phi^{(2)}}{\partial r}. \end{aligned} \tag{31}$$

By substituting (27) and (29) into (30), we obtain:

$$\sum_{j=1}^{4} M_{ij} B_j = 0, \quad i = 1, 2, 3, 4, \tag{32}$$

where

$$\begin{aligned} M_{1j} &= \left(2\tilde{c}_{11}^{(0)}\alpha_{1j} + 2\tilde{c}_{13}\alpha_{2j} - \tilde{c}_{11}^{(3)}\alpha_{3j} + \pi\tilde{e}_{31}^{(3)}\alpha_{4j}\right) J_0(\xi_j a) \\ &\quad - 4\tilde{c}_{66}\alpha_{1j}\frac{J_1(\xi_j a)}{\xi_j a}, \\ M_{2j} &= \left(\tilde{c}_{11}^{(2)}\alpha_{3j} - \tilde{c}_{11}^{(3)}\alpha_{1j} - \frac{2}{3}\tilde{c}_{13}\alpha_{2j} - \pi\tilde{e}_{31}^{(2)}\alpha_{4j}\right) J_0(\xi_j a) \\ &\quad - 2\tilde{c}_{66}\alpha_{3j}\frac{J_1(\xi_j a)}{\xi_j a}, \\ M_{3j} &= \left(\frac{3}{8}\tilde{c}_{55}^{(1)}\alpha_{2j}X_j^2 - \frac{4}{\pi^2}\alpha_{3j} + \frac{1}{\pi}\tilde{e}_{15}\alpha_{4j}X_j^2\right)\frac{J_1(\xi_j a)}{\xi_j a}, \\ M_{4j} &= \left(-\frac{8}{3\pi}\tilde{e}_{15}\alpha_{2j}X_j^2 + \tilde{\epsilon}_{11}\alpha_{4j}X_j^2 + \frac{4}{\pi}\tilde{e}_{15}\alpha_{3j}\right)\frac{J_1(\xi_j a)}{\xi_j a}. \end{aligned} \tag{33}$$

The vanishing of the determinant of the coefficient matrix M_{ij} of (32) gives the frequency equation for the E-TSt-s.TSh vibrations of circular disks of piezoelectric ceramics, i.e.:

$$F\left(\Omega, \frac{a}{b}\right) = \det[M_{ij}] = 0. \tag{34}$$

The resonance frequencies of the first 11 modes for $BaTiO_3$ disks with the diameter-to-thickness ratio (a/b) up to 20 are numerically calculated from (34) and plotted as solid lines in Fig. 3.The experimental data of Shaw [4], which are extracted from Fig. 10 of [4] and converted to the dimensionless frequency Ω, defined in (24), by using the shear-wave velocity [5]:

$$v_2 = \sqrt{\frac{c_{55}}{\rho}} = 2690 \text{ m/sec}, \tag{35}$$

are plotted as dots in Fig. 3 for comparison.

Fig. 3 shows very good general agreement between the experimental data and the theoretical results, including the frequencies of edge modes. In [5] the theoretical frequency of edge modes is lower than the experimental value by about 12%; the discrepancy in Fig. 3 is less than 3%. As discussed in [5], the most likely cause of the discrepancy seems to be that the details of the complex segments of the dispersion curves become important in the neighborhood of the frequency of the edge modes. As shown in Fig. 2, the imaginary part of the complex segments calculated from the present 2-D equations agrees very closely with that from the 3-D equations, and the agreement between the real parts is only fair. Nevertheless, the overall agreement is better than the 2-D theory in [5], thus the present 2-D equations provide closer prediction in the frequency of the edge mode.

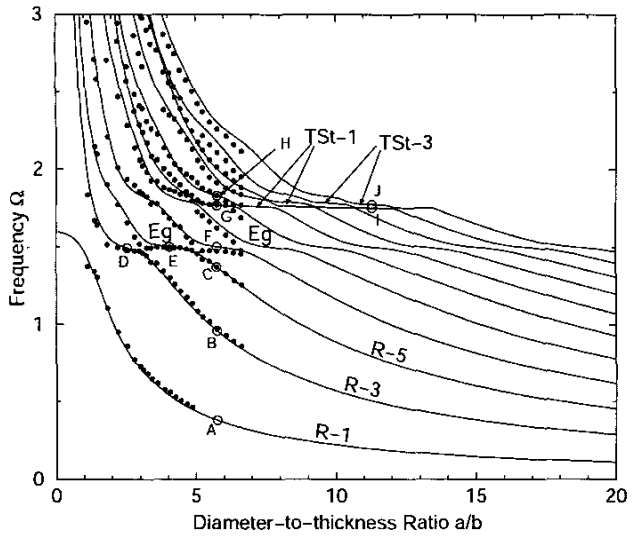

Fig. 3. Frequency Ω vs. diameter-to-thickness ratio a/b of $BaTiO_3$ disks. Solid lines are predicted from the 2-D equations, and the solid dots are experimental data of Shaw.

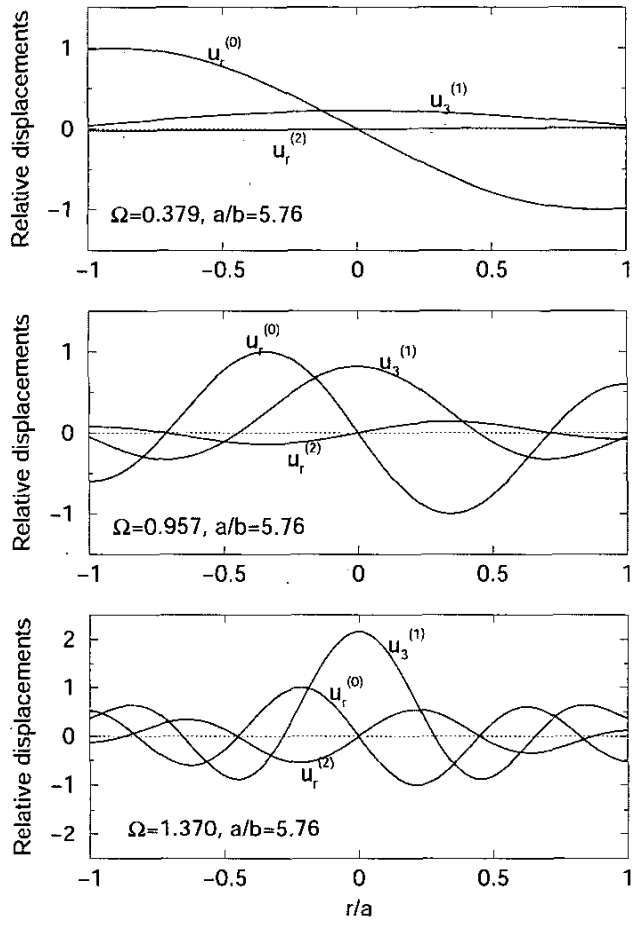

Fig. 4. Distribution of displacements along a diameter of a $BaTiO_3$ disk with $a/b = 5.76$ at frequencies corresponding to points A, B, and C in Fig. 3.

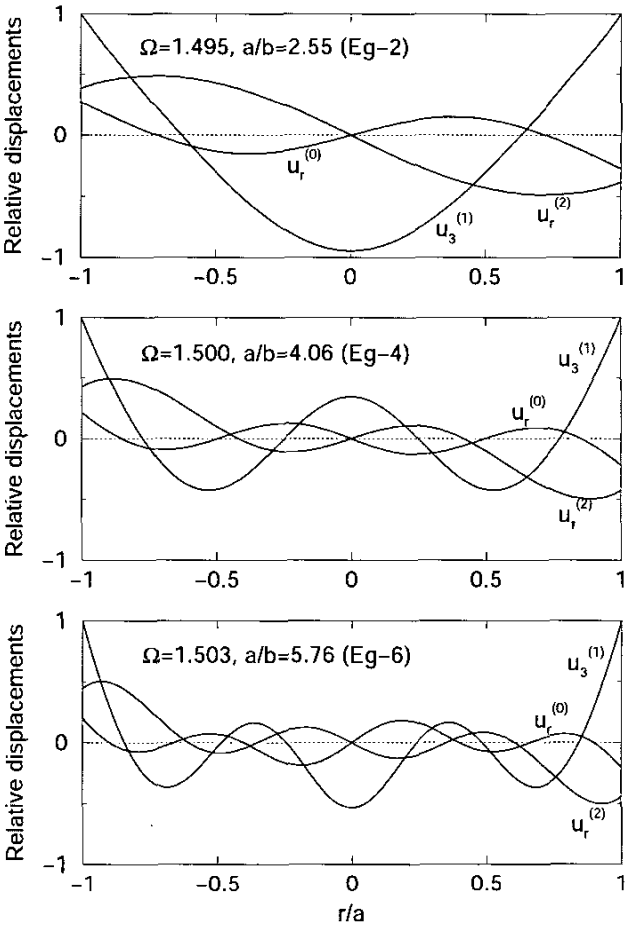

Fig. 5. Distribution of displacements along a diameter of $BaTiO_3$ disks for the edge modes Eg-2, Eg-4, and Eg-6 at frequencies corresponding to points D, E, and F in Fig. 3.

In order to understand the patterns of vibrations at various locations of the spectrum in Fig. 3, mode shapes at resonance frequencies are calculated from (27) and (29) by obtaining the amplitude ratios of B_j from (32). Fig. 4 shows the distribution of relative displacements along a diameter of a circular disk of $BaTiO_3$ with $a/b = 5.76$ at frequencies corresponding to the points A, B, and C in Fig. 3. Fig. 4 shows the radial displacement $u_r^{(0)}$ is predominant at $\Omega = 0.379$. As Ω increasing, the amplitude of the thickness-stretch displacement $u_3^{(1)}$ increases and becomes greater than that of $u_r^{(0)}$ at $\Omega = 1.370$. Therefore, the segments of the first three frequency branches at low frequency and large a/b ratio in Fig. 3 are identified as predominantly radial extensional modes R-1, R-3, and R-5, in which the integers denote the number of nodes of $u_r^{(0)}$ across the diameter of the disk.

Fig. 5 shows the distribution of relative displacements at $\Omega \approx 1.5$ for disks with $a/b = 2.55$, 4.06, and 5.76, corresponding to the points D, E, and F in Fig. 3, respectively. We see in Fig. 5 that $u_3^{(1)}$ is predominant and has large amplitude at the edge of the disks. Hence, they are the edge

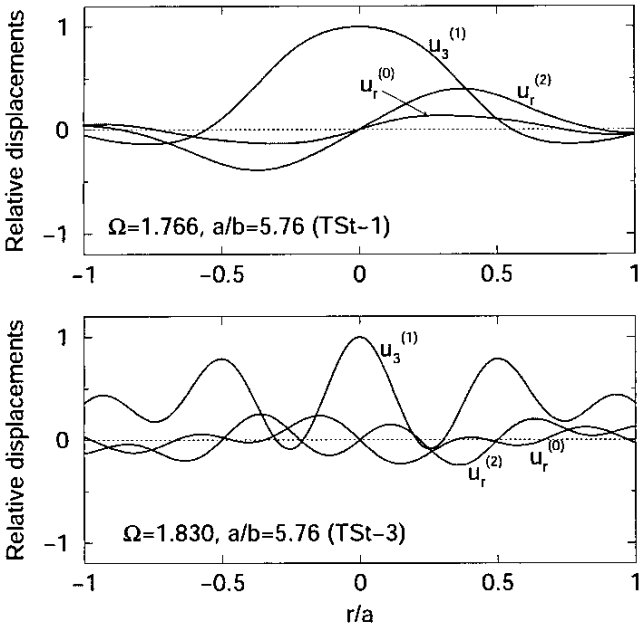

Fig. 6. Distribution of displacements along a diameter of a $BaTiO_3$ disk with $a/b = 5.76$ for the fundamental thickness-stretch mode TSt-1 and its third anharmonic overtone TSt-3 at frequencies corresponding to points G and H in Fig. 3.

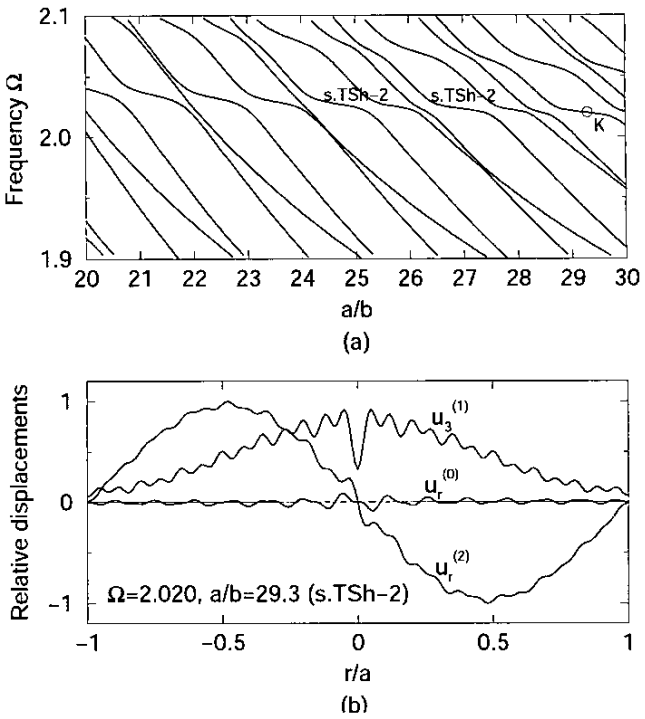

Fig. 8. (a) Frequency spectrum of $BaTiO_3$ disks for $20 < a/b < 30$ and $1.9 < \Omega < 2.1$; (b) Distribution of displacements for the symmetric thickness-shear mode s.TSh-2 corresponding to the point K in (a).

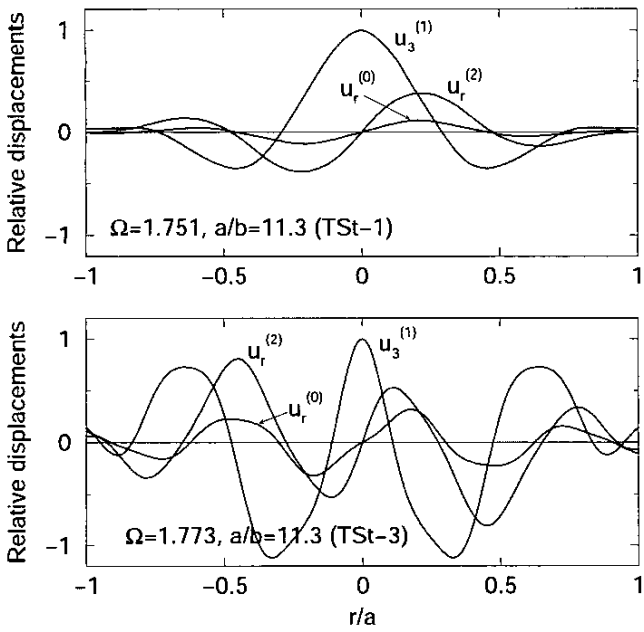

Fig. 7. Distribution of displacements along a diameter of a $BaTiO_3$ disk with $a/b = 11.3$ for the TSt-1 and TSt-3 modes at frequencies corresponding to points I and J in Fig. 3.

modes of thickness-stretch deformation $u_3^{(1)}$ and denoted by Eg-2, Eg-4, Eg-6 in Figs. 3 and 5, where the integers denote the number of nodes of $u_3^{(1)}$ across the diameter.

Usually, the terrace-like structure in a frequency spectrum begins at the frequency near the cut-off frequency of the corresponding mode. In Fig. 3, we see that the terrace-like structure starts near $\Omega = 1.75$, which is the cut-off frequency of the TSt mode at nonzero wave number as shown in Fig. 2. Displacements of the fundamental thickness-stretch mode (TSt-1) and its third anharmonic overtone (TSt-3) of a disk with $a/b = 5.76$ at frequencies indicated by points G and H in Fig. 3 are shown in Fig. 6. Similar plot is given in Fig. 7 for a disk with $a/b = 11.3$ at frequencies corresponding to points I and J in Fig. 3. By comparing the mode shapes in Figs. 6 and 7, it is seen that, for the thinner disk, the coupling of $u_3^{(1)}$ with other displacement components is stronger, and the mode identification becomes less certain. The distributions of $u_3^{(1)}$ shown in Figs. 4, 5, and 6 corresponding to the points B, C, D, E, F, G, and H are compared with Shaw's measured ones [4] with close agreement.

It is interesting to note that, in Fig. 3, there is no additional terrace-like structure for TSt mode near its cut-off frequency at zero wave number, $\Omega \approx 1.85$ (see Fig. 2). However, a terrace-like structure corresponding to the s.TSh mode does exist near its cut-off frequency at zero wave number, $\Omega \approx 2$ (see Fig. 2), but it is outside the range of a/b in Fig. 3. The portion of the spectrum

that includes the terrace structure for the s.TSh mode is shown in Fig. 8(a), and the mode shape corresponding to the point K in Fig. 8(a) is given in Fig. 8(b). In Fig. 8(b), the predominant mode is $u_r^{(2)}$ and denoted by s.TSh-2.

VI. Conclusions

The newly extracted second-order 2-D equations for extensional, thickness-stretch and symmetric thickness-shear vibrations of piezoelectric ceramic plates with electroded faces are shown to give accurate dispersion relations without any corrections as they are compared with those from the 3-D equations. Predicted resonance frequencies of circular disks of $BaTiO_3$ agree closely with the experimental data of Shaw [4], including the frequencies of the edge modes. By examining the mode shapes at various frequencies and a/b ratios, predominant modes are identified at various segments of the frequency branches of the spectrum.

References

[1] P. C. Y. Lee, J. D. Yu, and W. S. Lin, "A new two-dimensional theory for vibrations of piezoelectric crystal plates with electroded faces," *J. Appl. Phys.*, vol. 83, no. 3, pp. 1213–1223, 1998.

[2] P. C. Y. Lee and N. P. Edwards, "Extensional vibrations of piezoelectric crystal plates and strips," in *Proc. Joint Meeting Eur. Freq. Time Forum and IEEE Int. Freq. Cont. Symp.*, 1999, pp. 754–757.

[3] J. D. Yu, "Second-order analysis of free vibrations of piezoelectric ceramic actuators," in *Proc. IEEE Int. Freq. Contr. Symp.*, 1998, pp. 695–702.

[4] E. A. G. Shaw, "On the resonant vibrations of thick barium titanate disks," *J. Acoust. Soc. Amer.*, vol. 28, no. 1, pp. 38–50, 1956.

[5] D. C. Gazis and R. D. Mindlin, "Extensional vibrations and waves in a circular disk and a semi-infinite plate," *J. Appl. Mech.*, vol. 27, pp. 541–547, 1960.

[6] D. A. Berlincourt, D. R. Curran, and H. Jaffe, "Piezoelectric and piezomagnetic materials and their function in transducers," in *Physical Acoustics*. vol. I(A), W. P. Mason, Ed. New York: Academic, 1964, pp. 169–270.